Thermally induced phase separation in supported bilayers of glycosphingolipid and phospholipid mixtures

Alan W. Szmodis and Craig D. Blanchette
Biophysics Graduate Group, University of California, Davis, California 95616

Marjorie L. Longo
Department of Chemical Engineering and Materials Science and Biophysics Graduate Group, University of California, Davis, California 95616

Christine A. Orme
Biosciences and Biotechnology Division, Lawrence Livermore National Laboratory, Livermore, California 94551

Atul N. Parikh[a]
Department of Applied Science and Biophysics Graduate Group, University of California, Davis, California 95616

The authors have studied microstructure evolution during thermally induced phase separation in a class of binary supported lipid bilayers using a quantitative application of imaging ellipsometry. The bilayers consist of binary mixtures consisting of a higher melting glycosphingolipid, galactosylceramide (GalCer), which resides primarily in the outer leaflet, and a lower melting, unsaturated phospholipid, 1,2-dilauroyl-sn-glycero-3-phosphocholine (DLPC). Three different bilayer compositions of GalCer/DLPC mixtures at 35:65, 20:80, and 10:90 molar ratios were cooled at controlled rates from their high-temperature homogeneous phase to temperatures corresponding to their phase coexistence regime and imaged in real time using imaging ellipsometry. During the thermotropic course of GalCer gelation, we find that two distinct types of morphological features modulate. First, the formation and growth of chain and fractal-like defects ascribed to the net change in molecular areas during the phase transition. The formation of these defects is consistent with the expected contraction in the molecular area during the liquid crystalline to gel-phase transition. Second, the nucleation and growth of irregularly shaped gel-phase domains, which exhibit either line-tension dominated compact shape or dendritic domains with extended interfaces. Quantifying domain morphology within the fractal framework reveals a close correspondence, and the quantization of the transition width confirms previous estimates of reduced phase transition cooperativity in supported bilayers. A comparison of domain properties indicates that thermal history, bilayer composition, and cooling rate all influence microstructure details including shapes, sizes, and distributions of domains and defects: At lower cooling rates and lower GalCer fractions compact domains form and at higher GalCer fractions (or at higher cooling rates) dendritic domains are evident. This transition of domain morphology from compact shapes to dendritic shapes at higher cooling rates and higher relative fractions of GalCer suggests kinetic control of shape equilibration in these phospho- and glycolipid mixtures. © *2010 American Vacuum Society.* [DOI: 10.1116/1.3524295]

I. INTRODUCTION

Mechanisms of domain formation in phospholipid bilayers consisting of discrete number of components, e.g., binary and ternary mixtures, are of considerable scientific interest because they offer a window into understanding spatial distributions of membrane components in the living cell. The latter is an important goal because many important membrane functions, e.g., signaling and transport, appear strongly linked to their local microenvironment.[1–3] Specifically, important signaling molecules and transporter proteins either reside in or are recruited to specialized microdomains during their activated states.[4]

A basic hypothesis in understanding membrane domain formation is that they form via equilibrium or near-equilibrium phase behavior of membrane components. Specifically, (1) liquid-liquid immiscibility or phase coexistence,[5] (2) molecular complexation among specific membrane components,[6] (3) the solvation of microscopic lipid clusters within the fluid membrane solvent,[7] and (4) dynamic compositional fluctuations over a range of length and time scales[8] have all been invoked as plausible mechanisms for domain formation and stabilization. To compare and validate these notions, model phospholipid membranes, including Langmuir monolayers at air-water interface and giant unilamellar vesicles (GUVs), are proving quite valuable.[9–12] Studies based on these models are providing a physical-chemical basis for understanding the fundamental

---

[a] URL: http://parikh.ucdavis.edu; electronic mail: anparikh@ucdavis.edu

structural characteristics (e.g., sizes, lifetimes, and chemical compositions) and their relationships with many domain-mediated functions including protein recognition, membrane-mediated transport, and membrane permeability. It is notable that each of these model membrane configurations has its own merits and limitations. GUVs are closed equilibrated structures wherein lipids experience bulk water on either surface of the membrane bilayer. They equilibrate readily but cannot easily recapitulate compositional or structural asymmetry such as exists between the leaflets of cellular membranes. Langmuir monolayers at the air-water interface are similarly also at thermodynamic equilibrium, but being composed only of one leaflet, they cannot reconcile the role of interleaflet interactions, which exist in membrane bilayers.

But membrane components in biological cells often organize under active and/or spatiotemporally dynamic constraints.[13–15] For instance, interactions with the charged and dynamically rearranging cytoskeleton actively recompartmentalize the plasma membrane. Moreover, enzymes that maintain membrane asymmetry and dynamic readjustment of membrane compositions represent some of the additional active processes, which reshuffle membrane compositions and prompt membrane remodeling. While, GUVs and Langmuir monolayers have proved useful in characterizing equilibrium membrane phase behavior, influences of these dynamic perturbations and spatial compartmentalizations on phase separation and domain formation require different model systems.

To this end, single supported lipid bilayers (SLBs) (Ref. 16) offer a potentially useful alternative to model domain formation under externally constrained equilibration. SLBs are typically formed by rupture and spreading or fusion of small unilamellar vesicles (SUVs) at support surfaces.[17] While a very thin water layer, 0.6–1.5 nm thick,[18–20] present at the interface between the substrate and the bilayer is thought to cushion this interface, a growing body of evidence establishes that the physical-chemical character of the substrate surface influences bilayer properties either directly or by modulating the interfacial water layer. For instance, the physical proximity of the substrate limits the out-of-plane undulations and introduces an additional drag at the interface between the lower leaflet and the stationary substrate.[21,22] Using polymeric cushions and tethers, it appears possible to deliberately modulate these perturbations in a controlled manner.[23,24] Similarly, tailoring the charge, topography, and wettability of support surfaces (also in spatial arrays) provides additional means to produce (1) physical compartmentalization, (2) asymmetric leaflet-dependent distributions of charged lipids, and (3) even mono- and bilayer geometries in a predetermined manner. Thus, by tailoring support surfaces, extraneous constraints can be controllably introduced onto phase-separating lipid bilayers. Furthermore, understanding how membrane components phase separate in supported membranes is also important in its own right because of its

rapidly growing popularity in devising membrane based biomimetic devices and its use in many fundamental biophysical studies.[25,26]

In the present work, we study thermally induced phase separation of binary mixtures of a glycosphingolipid [galactosylceramide (GalCer), $T_m \sim 55\,°C$ depending on chain length] and a phospholipid [(1,2-dilauroyl-sn-glycero-3-phosphocholine (DLPC), $T_m = -2\,°C$], organized as supported lipid bilayers at oxided silicon surfaces. In this mixture, GalCer is the higher melting component, which undergoes preferential gelation when the mixture is plunged from a high-temperature homogeneous phase below GalCer's transition temperature. Our rationale for the selection of this mixture is based on several factors.[27] First, understanding the phase behavior of the bilayer mixtures of GalCer with phospholipids may have biological significance. GalCer has been implicated as a native receptor for gp120, an HIV-1 envelope glycoprotein. Using a variety of CD4 negative cells,[28–30] it has been demonstrated that gp120 and GalCer association becomes a primary mechanism for viral infection in CD4 deficient cells. Glycosphingolipid concentrations in these cell types have been found to be as high as 10%–20% of the total membrane lipid located primarily in the extracellular leaflet.[31] These concentrations may become even higher due to accumulation of glycosphingolipids when the production of galactocerebroside β-galactosidase, an enzyme responsible for hydrolyzing GalCer, is decreased such as during Krabbe disease.[32,33] At these high concentrations, GalCer is thought to exist in phase-separated domains in cellular membranes, which in turn may influence its interaction with gp120.[34,35] Indeed, a recent series of studies reveals the formation of large, microscopic GalCer-enriched domains in model lipid bilayers consisting of binary and ternary mixtures containing GalCer.[36–39] Second, both the high-temperature homogeneous phase and the regime of coexisting phases for GalCer/DLPC mixtures fall in an experimentally convenient range between 20 and 55 °C.[37,40] The modest temperatures required to thermally cycle the lipid mixture through GalCer's phase transition further reduce the risk of undesirable lipid oxidation or desorption from the supporting surface.

We have recently demonstrated the usefulness of imaging ellipsometry (IE) as a quantitative, large area, label-free, and real-time optical means to characterize phase transition dynamics and associated morphological changes in lipid bilayers supported on solid substrates.[41] The technique of ellipsometry simply measures the modulation of light polarization upon reflection from the sample surface in terms of ellipsometric angles, Δ and Ψ. These parameters relate to polarization dependent optical reflectivities through a simple relation: $\tan \Psi e^{i\Delta} = R_p/R_s$, where R_p and R_s represent Fresnel reflectivities for *p*- and *s*-polarization, respectively.[42] Described in detail previously,[41,43] IE offers an attractive alternative to widely used fluorescence and atomic force microscopy (AFM), because of its many unique features. First, in imaging mode, ellipsometry takes advantage of the spatial differences in the optical properties of coexisting surface

phases[44] making it a label-free method of investigation. Second, imaging ellipsometry affords large area sampling (over 2.75×10^5 μm^2), albeit at a lower lateral resolution (1–2 μm/pixel) than AFM, thus enabling more accurate statistical analyses. Third, ellipsometry is a nonperturbative method of obtaining film thicknesses with angstrom level resolution with relatively rapid scan times (1–2 s for contrast images and 1–10 min for thickness maps) when compared to AFM.

This study builds on our earlier communication in which ellipsometric visualization of morphological changes during phase transition dynamics using single supported lipid bilayers consisting of DLPC/GalCer mixtures was reported.[45] In this article, we focus on the details of microstructure evolution, which includes morphologies of domains and defects as functions of lipid compositions and cooling rates. To enable systematic comparisons, three different compositions of GalCer:DLPC bilayers, 35:65, 20:80, and 10:90 mol ratios, and multiple different cooling rates are employed. The dependence of domain shapes on cooling rates and GalCer composition reveals that shape equilibration of gel-phase domains requires composition-dependent threshold cooling rates.

II. EXPERIMENT

A. Materials

DLPC was obtained from Avanti Polar Lipids (Alabaster, AL) and GalCer (a mixture of hydroxylated and nonhydroxylated GalCer with tail lengths varying from 16 to 24 carbons) from Matreya (Pleasant Gap, PA; note: an estimate of tail length variations in GalCer is provided in Matreya Handbook). All lipids were suspended and stored in chloroform or chloroform/alcohol mixture in the freezer (−20 °C) until use. Hydrogen peroxide (30% v/v) and sulfuric acid were purchased from J. T. Baker (Phillipsburg, NJ) and Fisher Chemicals (Fairlawn, NJ), respectively, and used as received. All organic solvents were high-performance liquid chromatography grade. All chemicals were used without further purification. Organic-free de-ionized water of high resistivity (18.2 MΩ cm) was obtained by processing water first through a reverse osmosis de-ionization unit and then a Millipore Synthesis water filtration unit (Billerica, MA). Test-grade silicon substrates with native oxide overlayers (Silicon Sense, Nashua, NH) were used as solid supports.

B. Preparation of supported lipid bilayers

Lipid solutions in chloroform were combined to produce 35:65, 20:80, and 10:90 GalCer:DLPC mixtures. These were dried in a vial under a nitrogen stream, and placed under vacuum for ~2 h. Millipore water was then added to the dried lipid yielding a 0.5 mg/ml solution. The hydrated lipid solution was vortexed and then warmed in a bath sonicator to 55 °C. The warm solution was vortexed again and then placed in a tip sonicator. Tip sonication was performed for ~1–2 min, and the sonicated solution was allowed to cool. Vesicle fusion was carried out using 80 μl of the sonicated

solution administered on freshly oxidized silicon at room temperature. The lipid was allowed to incubate for 15 min. Samples were then rinsed with copious amounts of Millipore water in a large dish. Prior to vesicle fusion, silicon oxide substrates were freshly oxidized using a freshly prepared 4:1 (v/v) mixture of sulfuric acid and hydrogen peroxide. They are immersed in the solution for 4–5 min maintained at 90–110 °C (caution: this mixture reacts violently with organic materials and must be handled with extreme care). The substrates were then withdrawn using Teflon tweezers, rinsed immediately with copious amount of water, and stored under vacuum prior to use. Directly before use, the silicon substrates were plasma cleaned (Harrick Plasma, Ithaca, NY) for 3 min, rinsed with water, and again dried under a nitrogen stream.

C. Thermal cycling experiments

As-prepared samples were annealed by placing in a 1 l crystallization dish of warm water maintained at 55 °C in an oven. The oven was then turned off and the samples allowed to cool overnight. To cool samples at a faster rate, samples were placed in a smaller dish of heated water (0.3 l) and allowed to cool at controlled cooling rates. Samples were placed in a fluid cell after cooling for aqueous ellipsometric characterization. Samples sets were also placed directly in the imaging fluid cell after membrane formation for real-time ellipsometric imaging during heating and cooling cycles. Heating of the fluid cell was controlled by a circulation water bath (Isotemp 3013, Fisher Scientific, Pittsburgh, PA) connected to flow ports in the base of the fluid cell, but separate from the sample portion of the cell. The temperatures of the samples in the crystallization dishes and in the fluid cell were monitored using K-type thermocouples connected to a computer for data storage.

D. Imaging ellipsometry

Ellipsometric angles, Δ and Ψ, and spatially resolved ellipsometric contrast images were acquired using a commercial Elli2000 imaging system (Nanofilm Technologie, Göttingen, Germany). The ellipsometer employed a frequency-doubled Nd:YAG (yttrium aluminum garnet) laser (adjustable power up to 20 mW) at 532 nm and equipped with a motorized goniometer for an accurate selection of the incidence angle and corresponding detector positions. The ellipsometer employed the typical polarizer-compensator-sample-analyzer nulling configuration in which a linear polarizer (P) and a quarter-wave plate (C) yields an elliptically polarized incident beam. Upon reflection from the sample (S), the beam is gathered via an analyzer (A) and imaged onto a charge-coupled device (CCD) camera through a long working distance 10$\times$ objective. The P, C, and A positions that yield the null condition are then converted to the ellipsometric angles, Δ and Ψ. Measurements were taken at an incidence angle of 60°. Silicon substrates with a native oxide overlayer (SiO$_2$/Si) whose surface chemistry is comparable to that of glass were used to enhance the optical contrast with

the lipid phase. For characterization under aqueous conditions, a fluid cell was used (Nanofilm Technologie, Göttingen, Germany). The field of view and lateral resolution of the acquired images are limited by the objective and CCD (768×572 pixel resolution) used. The specified accuracy in ellipsometric angle determination is 0.01° for our instrument.

Typically, 70–140 contrast images were scanned incrementally over a 4°–8° change in polarization angle, while maintaining the analyzer angle at a constant value. These scans were then assembled to determine the null for each point comprised of a 2×2 region of pixels binned together. Δ values estimated for the individual null conditions were mapped two dimensionally using the micromapping feature of the ELLI2000 software.

E. Optical models for the determination of ellipsometric thickness

Ellipsometric data were analyzed using classical electromagnetic theory and a four-phase parallel-slab model each having its own index of refraction, n.[41] The sample model was approximated by semi-infinite slabs of silicon ($n = 3.875 + 0.018i$) and water ($n = 1.33 + 0i$) separated by an ~2 nm native silicon oxide layer ($n = 1.5 + 0i$) and the lipid bilayer slab of phase-state dependent optical constants.[46,47] Refractive index values were estimated from the optical properties of similar lipids under comparable conditions of molecular packing and phase state.[40,46,48]

For our single-wavelength measurements, the ellipsometry equations do not allow an independent determination of both the optical function and the thickness of the lipid bilayer from the values of ellipsometric angles, Δ and Ψ. Therefore, the film thickness was determined using independently assigned values for the substrate and film optical functions. Given the uncertainties associated with an accurate assignment of thickness and the dielectric constants for the head-group regions and hydration layer, we approximate the entire lipid layer as consisting of a single dielectric slab rather than approximating separate slabs for the head-group and tail regions.

Oriented acyl chains induce a small, but nonvanishing uniaxial anisotropy, which is highest for ordered chains in the gel phase and substantially lower for the fluid phase. Strictly, the optical constants should incorporate the uniaxial anisotropy due to phase-dependent average oriented structure of the acyl tails. In these measurements for bilayers supported on silica, however, the effects of optical anisotropy on thickness are estimated to be below 1%. If previous estimates[47] of $n_{\parallel} = (1.47, \text{fluid}; 1.51, \text{gel})$ and $n_{\perp} = (1.42, \text{fluid}; 1.57, \text{gel})$ are used, in conjunction with rigorous anisotropic optical calculations,[49] comparable values are obtained with the averages we have used of $n = (1.45, \text{fluid}; 1.53, \text{gel})$. While the 0.01° accuracy in Δ offers a substantial vertical resolution (< 0.02 nm), the approximation engendered in our model and sample to sample variabilities limit the accuracy of absolute measurements to ~0.1–0.2 nm.
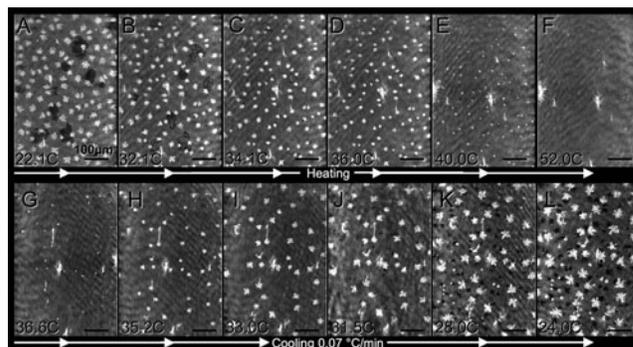
FIG. 1. Snapshots of a 20:80 cycle: ellipsometric contrast images (430×645 μm^2) of 20:80 GalCer:DLPC lipid bilayer on a Si/SiO$_2$ support during a heating-cooling cycle in a fluid cell. [(a)–(f)] Sample was heated causing domains to melt and [(a)–(c)] defects to diminish resulting in a continuous membrane. [(g)–(l)] Sample was cooled at 0.07 °C/min rate showing domain growth and [(j)–(l)] defect growth.

Ellipsometric thickness averages were determined by selecting several locations near the center of the calculated thickness maps for each sample. In cases where coexisting lipid phases of differing refractive indices were present, separate average thicknesses were measured for each phase. This required the calculation of separate thickness maps using a corresponding refractive index map.

III. RESULTS

A. Thermal cycling experiments

Figure 1 shows a sequence of ellipsometric contrast images chosen arbitrarily from a representative movie for a single supported lipid bilayer consisting of 20:80 GalCer:DLPC mixture during a thermal cycle between 55 and 22 °C. The bilayer was prepared by fusion of SUVs onto a freshly oxidized silicon wafer at 55 °C. The sample was then allowed to cool to room temperature in a water bath at a controlled, slow rate of 0.1 °C/min. Figure 1(a) shows an ellipsometric image of the cooled sample at room temperature before the subsequent heating-cooling cycle began. This frame shows a random distribution of bright irregularly shaped clusters uniformly covering the imaged area. These clusters are remarkably uniform in size and have an average area of ~350 μm^2. A closer inspection of the clusters reveals a pervasive fractal-like morphology. The image also displays some larger, dark irregular features. These features have an average size of 480 μm^2. The bright features represent structurally denser and taller regions within the bilayer whereas darker regions represent less dense, lean areas of the bilayer (see below, Sec. III B). Averaging over the image frame, we find that the structurally taller (or denser) clusters occupy roughly 18% and the less frequent dark features of lower bilayer density only 4% of the total average area sampled. Translating the image plane over millimeter distances throughout the sample revealed comparable populations of the bright clusters and dark features.

Upon heating, both of these features begin to decrease in size. At ~36 °C, the low-density darker features first disap-
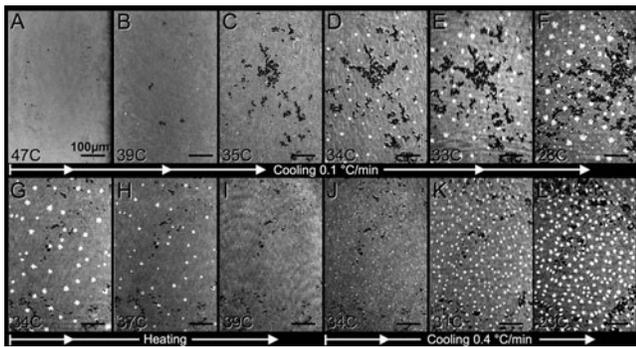
FIG. 2. Snapshots of a 35:65 cycle: ellipsometric contrast images (430 × 645 μm^2) of 35:65 GalCer:DLPC lipid bilayer on a Si/SiO$_2$ support during a cooling-heating-cooling cycle in a fluid cell. (a) Sample was cooled at 0.1 °C/min rate and begins to show low-density defects appearing as black regions, which [(b)–(f)] continue to grow into extended defect chains. (d) White GalCer domains appear and [(e) and (f)] continue to grow. [(g) and (h)] Sample is reheated, domains return to fluid state, and defects diminish in size. [(j)–(l)] Sample is cooled again at a faster rate of 0.4 °C/min. Domains reappear and grow with defects increasing in area. Data adapted from a previous communication (Ref. 45).

pear [Fig. 2(d)], while the taller (or denser) brighter regions continue to shrink with increasing temperature. Above ~43 °C, the tall clusters also disappear and sample reaches an optically homogeneous state as seen in Fig. 1(f). Throughout the heating process neither the denser bright spots nor the leaner dark features appear to diffuse or migrate relative to one another. After allowing the sample to stand at about 50 °C for ~40 min, the sample is cooled to room temperature at a comparable, but slightly lower rate of 0.07 °C/min [Figs. 1(g)–1(l)]. Bright fractal-like clusters begin to reappear at ~37 °C. Note that the spatial locations of the spots are different from those observed in the as-prepared sample. These spots continue to grow as temperature is lowered further, but the number of spots does not appear to increase at lower temperatures. At about 32 °C, small dark features of low density begin to appear. Both denser bright clusters and leaner dark features continue to grow until the lowest temperature of the thermal cycle of 24 °C is reached. As was seen during the heating cycle, no relative mobility of these features was visible. Note also that the temperature range (phase transition width) over which denser, bright clusters and the leaner, dark features form and grow is relatively broad spanning from 28 to 38 °C.

The end point image of the annealed sample [Fig. 1(l)] near room temperature (obtained after the heating sequence) is qualitatively similar to the sample image obtained for the as-prepared sample before the beginning of the thermal cycle [Fig. 1(a)]. This sample, however, has two distinct differences. First, the average sizes of the denser bright features in the annealed samples are somewhat larger at 450 μm^2 [compared with ~350 μm^2 in Fig. 1(a)] occupying comparable 17% [compared to 18% in Fig. 1(a)] of the frame. The leaner dark regions, however, average a much smaller size of 130 μm^2 [compared to 480 μm^2 in Fig. 1(a)] and now covering slightly larger 6% [compared to 4% in Fig. 1(a)] of the frame. These increases in sizes of denser clusters and leaner

defect structures observed at a lower cooling rate are not surprising since the latter should afford a closer approach to bilayer equilibration. These low-density darker features are also fractal-like in morphology and appear to preferentially form within a close vicinity of the denser bright spots— possibly suggesting incomplete equilibration (see Sec. IV). These features were reproduced in subsequent heating-cooling cycles.

Figure 2 summarizes selected ellipsometric contrast images from a cooling-heating-cooling thermal cycle for a 35:65 GalCer:DLPC bilayer. After vesicle fusion, as-prepared samples were first let to stand at a temperature of 55 °C for about 20 min before the first cooling sequence began. In this cycle, the sample was first cooled from an initial homogeneous state (formed after vesicle fusion) at 0.1 °C/min [Figs. 2(a)–2(f)] heated back up [Figs. 2(g)–2(i)], and again allowed to cool [Figs. 2(j)–2(l)], but at a faster rate of 0.4 °C/min. During cooling, the bilayer appears homogeneous [Fig. 2(a)] until reaching a temperature of about 39 °C [Fig. 2(b)]. At this temperature, small dark regions representing low-density leaner defectlike features in bilayers first become visible. These features grow as temperature is reduced further, ultimately forming extended chainlike structures occupying as much as 16% of the frame area at 28 °C. A scan of the sample over macroscopic areas revealed that the large area distribution of these chainlike structures was highly variable and its frame area varied between as little as 0% and as large as 16% seen in Fig. 2(f). At around 34 °C during this cooling sequence [Fig. 2(d)], bright fractal-like cluster features, similar to those observed for 20:80 GalCer/DLPC mixture described above, begin to appear. These bright clusters also grow as the sample is cooled further (along with the dark chainlike structures) [Figs. 2(d)–2(f)]. Here also, the temperature range over which the denser bright clusters form and grow in all cases is broad between 28 and 38 °C. Interestingly, at the lowest temperature of 28 °C, denser clusters are present in a bimodal distribution of domain sizes with average peaks around 100 and 700 μm^2. The larger clusters adopt a well-defined fractal-like shape, while the smaller feature morphologies are difficult to distinguish, since they are at the threshold of our spatial resolution (1 μm).

The sample was again reheated and the microstructure evolution during the process monitored [Figs. 2(g)–2(i)]. As temperature increases, first the leaner dark regions begin to shrink as was seen for the 20:80 mixture. This is followed by a gradual shrinkage of the denser bright clusters, which dissolve fully in the surrounding fluid phase at 39 °C. Unlike that observed in the 20:80 mixture, some remnant defectlike dark regions remained after the system was reheated. The sample was allowed to rest in the homogeneous state for ~20 min, during which time the imaged area shifted slightly. The second cooling was conducted at a faster rate of 0.4 °C/min. Images in Figs. 2(j)–2(l) summarize the second plunge into the miscibility gap. The bilayer again begins to form leaner dark regions that seemingly spawn from the pre-existing ones. Bright fractal-shaped clusters representing

dense features also reappear. Domains during this fast-cooling cycle are smaller and more monodisperse. Control samples, cooled in an oven under comparable conditions, showed similar morphologies.

Taken together, the thermal cycling experiments above demonstrate the type of microstructure evolution that follows the plunge of supported bilayers consisting of binary GalCer/DLPC compositions from their high-temperature homogeneous phase into the miscibility gap. The results show that the homogeneous morphology is reversibly abandoned in the miscibility gap. The microstructure is characterized by the coexistence of three morphologically distinct features, two of which are discrete domainlike in appearance, which modulate with temperature in a composition-dependent manner.

B. Determination of spatially resolved ellipsometric thickness map of phase-separated GalCer/DLPC bilayers

To determine the properties of the bright clusters and dark features observed in the phase-coexistence region of GalCer/DLPC bilayers, we first turn to quantitative analysis of the ellipsometric angles. The analysis involves an application of classical electromagnetic theory in conjunction with a parallel-slab representation of the sample to deduce optical thickness information from the ellipsometric data (see Sec. II for details).

The ellipsometric angles for the bilayer in the high-temperature homogeneous state were analyzed by assuming a uniform fluid phase refractive index of $1.45+0i$. This yields a uniform optical thickness of 4.1 ± 0.2 nm. Note that our simplified model does not accurately account for either the water layer between the membrane and the substrate or the differences in optical constants (or thicknesses) due to head-group hydration. Taking into account errors introduced due to these simplifications, our values agree well with those reported ($\sim 3-4$ nm) for uniform, single lipid bilayers of comparable lengths.[41]

In the phase-coexistence region, the ellipsometric angle Δ shows a substantial spatial variation. Figures 3(a) and 3(b) show a spatial map of Δ obtained for 20:80 and 35:65 GalCer/DLPC bilayers annealed at a slow cooling rate of 0.05 °C/min. Using a uniform optical constant of $1.50+0i$ for both domains and the surrounding bilayer regions, a preliminary thickness map shown in Figs. 3(c) and 3(d) is calculated. This analysis reveals that the fractal-like clusters are 4.6 ± 0.2 nm whereas the surrounding bilayer is 3.4 ± 0.2 nm. While strictly inaccurate, this simplified treatment provides an important first step toward phase assignments of the two observed morphologies, namely, brighter clusters and darker features, which modulate during the thermal cycle. The 4.6 nm thickness obtained for the brighter clusters is indicative of taller topological features. It confirms that the bright clusters seen in the ellipsometric contrast images in Figs. 1 and 2 are structurally denser or topographically taller features. Because GalCer is undergoing gelation in this window of temperatures, we can straightforwardly assign the dendritic clusters to GalCer-rich domains and the
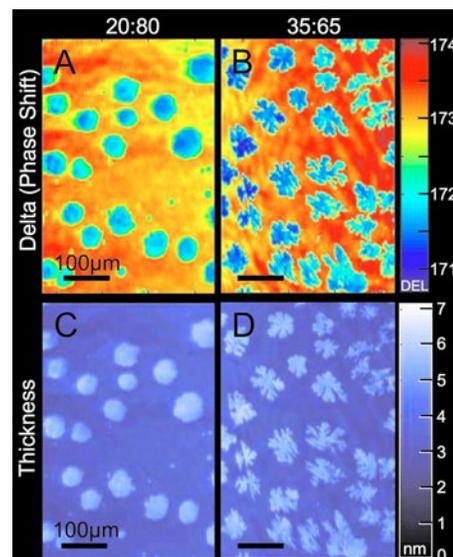

FIG. 3. (Color online) Delta and thickness maps: delta maps of slow cooled (0.05 °C/min) (a) 20:80 and (b) 35:65 displaying the differences in phase shift of light after interacting with sample. Thickness maps of (c) 20:80 and (d) 35:65 calculated from the delta maps above and a four-slab model using a refractive index of 1.50 for the bilayer region (see text for details).

surrounding phase to be a low melting DLPC-rich fluid. While darker features are mostly absent in the slow cooled (0.05 °C/min) samples seen in Fig. 3, thickness values for dark features have been calculated from Δ maps obtained from other sample areas. These darker features measure the thicknesses of 0.3 ± 0.1 nm and must then represent defect areas that are essentially voids in the membrane. A strict adherence to this average remnant thickness in the defect regions corresponds to a composition of approximately 5%–10% lipids.[50]

A more rigorous analysis of ellipsometric angles [Figs. 3(a) and 3(b)] requires the use of separate refractive indices for different phases. Note that the effects of uniaxial anisotropy of lipids in our samples (below 1%) were determined to be too small to require more rigorous anisotropic modeling. Because the brighter clusters in ellipsometric images appear and grow in the phase coexistence region as the sample temperature is lowered, it seems reasonable that they correspond to the incipient condensed phase formed due to GalCer gelation. To obtain more accurate thickness values, separate optical constants were assigned to the dense phase (GalCer-rich) domains ($n=1.53+0i$) and the surrounding DLPC-rich fluid phase ($n=1.45+0i$) based on previous estimates of typical glyco- and phospholids in their gel and fluid phases respectively.[40,46,48] These calculations yield thickness values of 4.5 ± 0.1 nm for the domains and 3.6 ± 0.2 nm for the surrounding bilayer. While a direct verification of the absolute values is not available from prior literature, the height disparity of ($4.5-3.6=0.9$ nm) between the GalCer-rich domains and the DLPC-rich surrounding is in excellent agreement with a recent AFM estimate of ~ 0.9 nm.[37]

To further characterize the dendritic character of the GalCer-rich domains, we quantify their fractal dimension us-
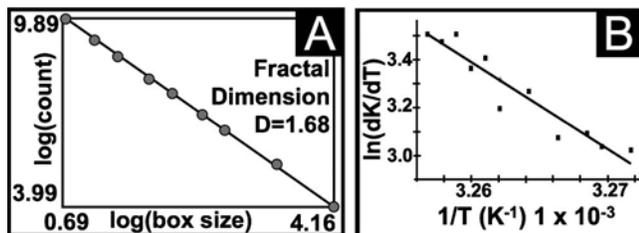
FIG. 4. Fractal dimension and enthalpy calculation: (a) a dimensional analysis of Fig. 3(d) using a box-counting logarithmic plot of box size versus count. A slope calculation yields the average fractional dimension of 1.68. (b) Temperature dependence of degree of phase transition estimated from ellipsometric data in Figs. 2(a)–2(f). $d\theta/dT$ represents the ratio of fluid area to solid area for a given temperature (see text for details).

ing the classical box-counting approach. Here, the object of interest or the domain is fitted with smaller boxes of variable sizes s. If $N(s)$ is the number of boxes of size s required to fill the original object, then the dimensionality D of the object can be estimated from a simple relation $N(s)=(1/s)^D$. Taking the logarithm of both sides and plotting $\log(N(s))$ against $D \log(1/s)$ yield the object's dimension D. Precise values of D reflect the topology of the object. Noninteger values of D represent fractional (fractal) dimension associated with self-similar fractal-like structures. As seen in Fig. 4(a), performing this analysis for a randomly chosen domain in Fig. 3(d) (NIH Image J) yields the fractal dimensions (D) of 1.68. Repeating this analysis across all domains observed in Fig. 3(d) yields an average fractal dimension of 1.63 with a narrow standard deviation of 0.08 about this value. These values compare well with $D=1.67$ derived previously for a triangular lattice of particles undergoing classical diffusion-limited aggregation in two dimensions.[51,52]

In summary, the analysis of ellipsometric angle Δ establishes that the bright clusters seen in ellipsometric contrast images correspond to structurally taller and denser GalCer-rich regions, and the dark features have vanishing thickness values indicative of the formation of defects or voids in the supported bilayers following their plunge into the phase coexistence region.

C. Transition enthalpy and cooperativity determination

It is instructive to note that the structure evolution seen in Figs. 1 and 2 occurs over a rather broad range of temperatures. For both compositions (20:80 and 35:65 GalCer/DLPC), the changes in sizes of GalCer rich domains and defects occur continuously between 28 and 38 °C. Previous studies suggest that the heterogeneous mixture of chain length and unsaturation alone cannot fully explain this large transition width.[53] Analyzing the temperature dependence of this fluid-gel transition in terms of the van't Hoff formalism provides useful insight such as given below.

It is reasonable to assume that the relative area fraction of the gel to the fluid phase at a given temperature within a transition window represents its equilibrium constant $K_{eq} = A_{liq}/A_{gel}$. Thus, according to the classical van't Hoff equa-

tion, the temperature dependence of K_{eq} yields the enthalpy H associated with the gel-fluid transition of GalCer within a DLPC matrix, which can be written as

$$\frac{d \ln K_{eq}}{dT} = \frac{\Delta H}{RT^2}, \tag{1}$$

where R is the gas constant. Plotting the degree of transition in the van't Hoff form of $\ln(dK_{eq}/dT)$ against $1/T$ allows for the enthalpy of transition to be calculated from the slope of a best fit line to these points. Figure 4(b) is a plot of the relative areal amounts of fluid lipid to gelated lipid as a function of inverse temperature for the 35:65 mixture cooling cycle displayed in Figs. 2(a)–2(f). The relation of the slope of the line to the transition enthalpy is expressed as $m=-\Delta H_{vH}R$, which is calculated in this plot to be -3.6×10^4. Using this slope value, the transition enthalpy is subsequently calculated to equal $3\pm1\times10^5$ J mol^{-1}. This value is significantly larger when compared to those found in our own calorimetry studies for this mixture in concentrated bulk vesicular state $(2.5\times10^4$ J mol$^{-1})$.[45] This order of magnitude difference in values perhaps can be reconciled in terms of the transition, namely, the degree of cooperativity.

Cooperativity of phase transition represents the size of the cooperative unit undergoing phase change.[54] Typically for large crystals, an infinitely narrow transition is observed where at some standard temperature and pressure a bulk transition occurs. With this consideration, finite values of cooperativity reflect the coexisting phase morphology during phase transition and further reflect contributions from small ensemble sizes, which destroy perfect (infinitely narrow) cooperativity.

Using theories of cooperativity[55] based on the coexistence of clusters of lipid molecules, the degree of cooperativity was calculated for the 35:65 mixture. Considering the system to have three phases during phase transition, fluid (f), gel (s), and boundary phases (i) and the variations in statistical weights of these phases allow for the description of degree of transition (K). This is done using the classical Zimm and Bragg model[55]

$$K = \frac{1}{2}\left[1 + \frac{s-1}{\sqrt{(s-1)^2+4\sigma s}}\right]. \tag{2}$$

The parameter $s=\exp(-F_f/RT)$, where F_f is the free energy of the fluid state, reflects the temperature dependence of the statistical weight of the fluid clusters; and the cooperativity parameter ($\sigma=\exp(-F_i/RT)$), where F_i is the free energy of the interfacial state, arises from the interfacial free energy that tends to reduce the number of boundary phase molecules. A Taylor series expansion of s about the transition temperature then becomes

$$s \simeq 1 + \frac{\Delta H_t}{RT^2}(T-T_t). \tag{3}$$

Differentiating K with respect to T shows a linear dependence on $1/T$ around T_t with a negative slope from which σ may be determined. The temperature dependence of the degree of transition is then given by

$$\frac{dK}{dT} = \frac{1}{4\sqrt{\sigma}}\frac{\Delta H_t}{RT^2}, \qquad (4)$$

where H_t is the transition enthalpy. This is related back to the van't Hoff form, when the phase transition is considered a pseudounimolecular reaction as has been done above. The effective reaction enthalpy is then expressed as $\Delta H_{vH} = (1/\sqrt{\sigma})\Delta H_t$.[54] GalCer phase-change progression is determined by addition of GalCer clusters acting in concert and involving $1/\sqrt{\sigma}$ molecules, or the size of the cooperative unit.[54]

We consider the size of the cooperative unit involved in cluster formation using enthalpies determined through calorimetry and through ellipsometric image analysis during GalCer/DLPC membrane cooling. This comparison with the measured calorimetric transition enthalpies for galactocerebrosides (H_t ranging from 1.5 to 6×10^4 J mol^{-1})[45,53] and the ΔH_{vH} ($3 \pm 1 \times 10^5$ J mol^{-1}) determined from the plot [Fig. 4(b)] shows that $1/\sqrt{\sigma}$ or the cooperative unit is between 5 and 20 outer leaflet GalCer molecules. In comparison with previous studies that observed phase transition in single-component vesicles[54] and one-component supported bilayers,[56] these values are well within the range of these previous studies' estimates of 15–43 and 9–38 molecules, respectively.

D. Cooling rate and concentration dependence of GalCer domain and defect structure formation

To examine the kinetic effects in controlling the morphologies of domains and defects, we study the effects of cooling rates for three different bilayer compositions. Figure 5 compares room temperature ellipsometric contrast images of GalCer:DLPC bilayers consisting of three different compositions (GalCer:DLPC, 10:90, 20:80, and 35:65) at two different cooling rates (0.1 and 0.05 °C/min). The images also summarize the domain statistics in terms of percentage of area coverage by domains, average domain size, and number of domains for the frames shown. There are several noteworthy features in these data.

First, at the lowest cooling rate of 0.05 °C/min used in our study, the number of domains is the smallest for all three compositions tested. For instance, the number of domains for the 10:90 mixture [Figs. 5(a) and 5(b)] is half as many as that of the faster cooling rate. Similarly, there is about a fifth the number of domains for the more slowly cooled samples for the 20:80 [Figs. 5(c) and 5(d)] and 35:65 [Figs. 5(e) and 5(f)] mixtures compared to their faster cooled counterparts. Second, the average size of GalCer domains is substantially larger for slower cooling rates. This is further illustrated in a histogram of domain sizes for 35:65 samples measured at three different cooling rates of 0.4, 0.1, and 0.05 °C/min (Fig. 6). This demonstrates that there is a dramatic and nonlinear increase in domain area as the cooling rate decreases ranging from average area values of 130 to 1690 μm^2. Additionally, the corresponding polydispersity in domain sizes becomes lower as cooling rate decreases as can be most clearly seen in Fig. 5(e). Statistically, this appears as two
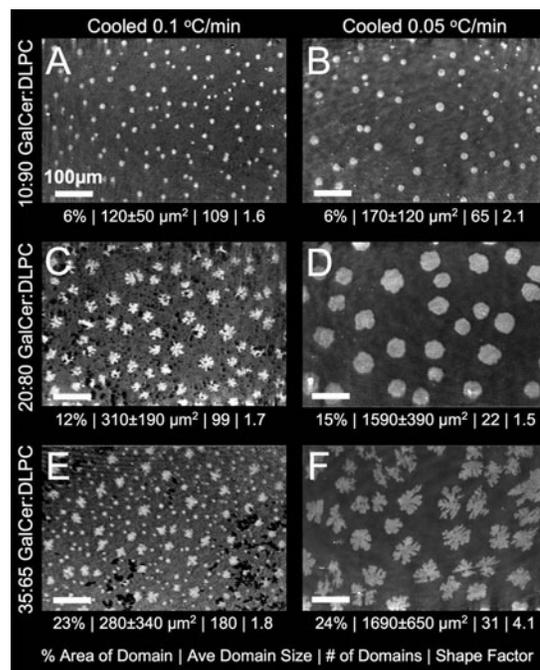

FIG. 5. Statistical comparisons: GalCer:DLPC lipid mixture concentrations of [(a) and (b)] 10:90, [(c) and (d)] 20:80, and [(e) and (f)] 35:65 on a Si/SiO$_2$ support compared at two different cooling rates: [(a), (c), and (e)] 0.1 °C/min and [(b), (d), and (f)] 0.05 °C/min. Each image is an ellipsometric contrast image 430×645 μm^2 taken after sample cooling at room temperature. Gel-phase GalCer domains appear as white against dark gray predominantly DLPC fluid membrane. Associated with each image in the center of the figure are the area % taken by the GalCer domains, average domain area, and the number of domains in the frame. Three general trends are revealed. (1) Domain size increases with GalCer concentration. (2) Slower cooling rate for a given concentration yields larger domains. (3) Faster cooling rate yields larger number of domains and domain size distribution for a given concentration. Data adapted from a previous communication (Ref. 45).

separate frequency peaks for two distinct domain areas as seen in Fig. 6 for the 0.1 and 0.4 °C/min samples. The net amount in the gel phase also appears to be dependent on composition but not on the cooling rate with these samples (Fig. 5) varying by at most 3% difference in total domain area for a given concentration, but different cooling rate. Third, the percent area covered by the domain regions increases with increasing GalCer concentration. However, a careful comparison suggests that the fractional area does not
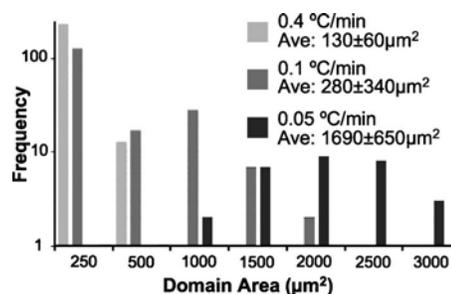

FIG. 6. Domain size histograms: histogram of GalCer domain size distributions at three cooling rates for a 36:65 GalCer/DLPC bilayer (see text for details).

match the molar ratio of GalCer:DLPC. The total domain area typically measures about 10%–30% less than the stoichiometric percent, assuming all GalCer to be in the outer leaflet and to have decreased by 15%–20% in area during phase change.[57] Fourth, as the concentration of GalCer increases so does the extent of defect formation. Samples of 10:90 mixtures show scant amounts of membrane defects within the limits of resolution, while higher GalCer containing samples reach defect area percentages as high as 16%. Finally, we find that at lower GalCer concentrations the domain morphologies are visibly more compact with mostly rounded domain perimeters.

In sum, the strong cooling rate dependence is observed in the precise microstructure, namely, domain number density, domain sizes, and defects, consistent with the general features of diffusion dependent processes.

IV. DISCUSSION

Compositional heterogeneities in biological membranes typically involve constrained phase separation between coexisting liquid phases.[12] Phase separations of solid-fluid type, such as examined here, are probably rare in biological membranes, but occur in many membrane components and their mixtures. For instance, they exist in the close vicinity of T_m in single-component lipid bilayers or over a larger temperature interval in many binary or multicomponent lipid mixtures (sans cholesterol), such as in mixtures of lipids of significantly different acyl-chain lengths, degree of saturations, or head-group types. The stable phase coexistence emerges in lipid mixtures when their high-temperature homogeneous phase is cooled to below the T_m of at least one of the mixture components. Such phase separations in lipid bilayers induced by selective phase transitions reflect a complex interplay between the energetics and kinetics due to the incipient phase change in the higher melting component, differences in relative lateral mobilities of the new and old phases, and the effects of the emergent phase on the residual fluid.[58]

The results presented in this study illustrate such thermally induced phase separation in single planar lipid bilayers supported at solid surfaces. We used a binary mixture consisting of a higher melting GalCer and a fluid DLPC with low T_m. Note that GalCer used in the present study itself is a multicomponent mixture of hydroxylated and nonhydroxylated species with acyl-chain lengths spanning a range between 16 and 24 carbons. However, the large disparity in the transition temperatures of DLPC and GalCer coupled with strong head-group driven propensity for the phase separation of GalCer from the DLPC phospholipid provides a reasonable rationale for its characterization as a binary mixture. When this bilayer is cooled from its high-temperature homogeneous liquid state into the solid-liquid coexistence region characterized by the gelation of higher melting GalCer, thermal cycling experiments presented for two different compositions of GalCer/DLPC bilayers confirm the reversible formation of the GalCer-rich domains and essentially lipid-free defects in the phase coexistence regime in rate and composition-dependent manners.

A. Domains

GalCer-enriched gel-phase domains observed in the miscibility gap regime reveal a characteristic dendritic shape (Fig. 3) at high GalCer concentrations. Qualitatively similar dendritic shapes have been reported previously for comparable GalCer:DLPC (60:40 molar ratio) bilayers supported on mica, with one notable difference. The domain sizes we observe are considerably larger over 60 μm compared with those of about 25 μm observed when bilayers were formed under comparable cooling rates. We surmise that this disparity in size reflects differences in substrate-membrane interactions due to differences in the charge and roughness of silicon and mica.

The growth process for the GalCer-enriched domains necessarily involves the diffusion of the gelating component from the fluid DLPC surroundings and its addition (also characterized as a binding reaction) to the existing ones. Thus, the thermally induced phase transition of GalCer and its attendant domain formation within their DLPC bilayer mixtures can be phenomenologically characterized as an example of two-dimensional diffusion-reaction processes. It is now well established that in such systems, the relative rates of diffusion, binding, and edge diffusion determine the growth morphologies.

The emergence of fractal-like morphologies during phase change provides some insights into the mechanism of gelation and its dependence on GalCer composition and cooling rate. Analogous growth morphologies form in diverse thin film structures including lipid monolayers at the air-water interface[59–62] and bilayers consisting of widely different lipid types, e.g., mixtures of diacetylenic lipids and phospholipids.[63] The extended phase boundaries of these domains suggest a slow edge diffusion compared to the rate of cluster growth likely reflecting high GalCer-GalCer interaction energy and low on-off rates during cluster formation and growth. Indeed, we find slow domain compaction over several hours when samples are maintained at fixed temperatures within the two-phase region. In this regard, our results also suggest that gel-fluid interfacial line tension, the force restoring minimum boundary length between the growing GalCer domains and the DLPC, is insufficient to produce compact domains. The fact that these fractal-like structures become more rounded after extended periods of time is an indication that they represent morphologies that are not shape equilibrated. Compact character of domains observed for 80:20 and 90:10 DLPC/GalCer compositions—especially at low cooling rates—also suggests that shape equilibration is strongly influenced by the relative fraction of gel-forming component and the cooling rate.

B. Defects

The formation of defects in the supported membrane is not surprising. As GalCer undergoes gelation, the areal shrinkage in GalCer must create density gradients. An analysis of the defect growth and area change allows us a window to determine the degree of membrane area change in a supported membrane as it is cooled. The defect area measure-

ments at a maximum of 16% of the sample surface area are indicative of at most a 16% shrinkage in the membrane area during cooling [Fig. 2(f)].

Previously in vesicle pipette aspiration studies,[57] Needham *et al.* demonstrated an area change in dimyristoylphosphatidylcholine (DMPC) upon the cooling of the system through a phase change. They also show that when membranes are tense the extent of membrane areal shrinkage reduces. For instance, DMPC vesicles without extraneous tension had an area change of 22% as the system moved across its phase boundary. However, by applying a moderate tension (0.2 dyn/cm) to the membrane and repeating the experiment, an area change of only 12% was observed. While it is unlikely that vesicles containing GalCer form large rips or defects,[37] we surmise that the degree of observed defect formation in our study may be due to residual tension in the supported membrane imposed by the substrate constraints. The tension added to the membrane via the silica support restricts the ability of the membrane to contract to a higher degree. Using the amount of membrane defects as a measure, we found the amount of membrane contraction to be in range with that observed in other studies of DMPC membranes on mica supports typically between 5% and 24%.[50,64]

The defect structure observed in the two compositions studied above suggests considerable differences. At 20:80, smaller fractal-like defects form in the vicinity of the domains possibly suggesting the effects of gelation on local microenvironment due to incomplete equilibration. In contrast, at 35:65 GalCer/DLPC compositions, the defects are extended chainlike structure with little or no correlation with the spatial distribution of GalCer-rich domains possibly indicating long-range collective deformation induced by gelation. Additionally, the 10:90 mixtures having small quantities of gelating lipid showed little to no defect formation on a length scale comparable to the imaging resolution. Selective gelation of GalCer plunges the binary lipid bilayer from a high-temperature homogeneous liquid phase into solid-liquid miscibility gap.

The supported membrane defects observed in this study not only have an interesting growth morphology, but may also yield insight into intra- and interleaflet dynamics. A first notable feature of these defects is that they are bilayer deep. Data from the calculated thickness maps measured a thickness of the defect regions of about 0.3 nm. This represents a scant amount of lipid remaining in either leaflet. Some recent studies suggest that distribution of GalCer is asymmetric between the two leaflets of supported bilayers derived by vesicle fusion on mica.[39,65] While it is plausible that such asymmetry may not be reproduced on silica substrates used in our study, it is nonetheless intriguing to compare the nature of defects we observe with the possibility that GalCer resides dominantly in the distal leaflet. On the basis of this assumption, if the gelation is concentrated in the distal leaflet, the appearance of bilayer-deep defects may indicate a concomitant restructuring of the inner leaflet. Such a scenario would be consistent with the notion that intralayer phase dynamics in one leaflet couple with the interlayer dy-

namics between the lipid leaflets.[66] Moreover, if GalCer resides in the distal leaflet and its gelation is removed from direct substrate interactions, this coupling of the two leaflets appears to be an intrinsic bilayer property rather than a substrate-induced effect predicted previously for symmetric bilayers.[67,68]

V. CONCLUSIONS

In summary, this work details the microstructure evolution and dynamics of thermally induced selective gelation of GalCer in the outer leaflet of single supported lipid bilayers consisting of DLPC:GalCer lipids at three different composition. During the extended thermal window of the phase transition, we find the modulation of two coattendant morphological features: the formation of chain and fractal-like defects related to the net change in molecular areas during the phase transition and the appearance of large microscopic domains. The two morphological features evolve over a wide temperature range, suggesting weak cooperativity and large intrinsic phase transition widths. Characterization of the defects reveals an interesting consequence of the interleaflet interactions. While the GalCer gelation occurs predominantly in the outer leaflet, the appearance of bilayer thick defects reveals that area shrinkage in one (distal) leaflet results in the reorganization of the other (proximal) leaflet. Furthermore, the comparison of domain properties as a function of the GalCer concentration and cooling rates reveals that shape equilibration is achieved only at the lowest cooling rates and for low fractions of gel-forming GalCer component. Under all other conditions, the dendritic shapes of the domains observed in the probe-free ellipsometric measurements confirm that the domain shapes do not result from the probe dynamics,[59] rather they reflect the diffusion dependence of GalCer gelation itself.

ACKNOWLEDGMENTS

[1] R. Welti and M. Glaser, Chem. Phys. Lipids **73**, 121 (1994).
[2] F. Maxfield, Curr. Opin. Cell Biol. **14**, 483 (2002).
[3] A. Laude and I. Prior, Mol. Membr Biol. **21**, 193 (2004).
[4] D. Lingwood and K. Simons, Science **327**, 46 (2010).
[5] H. McConnell and M. Vrljic, Annu. Rev. Biophys. Biomol. Struct. **32**, 469 (2003).
[6] S. Keller, A. Radhakrishnan, and H. McConnell, J. Phys. Chem. B **104**, 7522 (2000).
[7] Y. Hu, K. Meleson, and J. Israelachvili, Biophys. J. **91**, 444 (2006).
[8] O. Mouritsent and K. Jørgensen, Mol. Membr Biol. **12**, 15 (1995).
[9] V. von Tscharner and H. M. McConnell, Biophys. J. **36**, 409 (1981).
[10] E. London, Curr. Opin. Struct. Biol. **12**, 480 (2002).
[11] S. Mukherjee and F. Maxfield, Annu. Rev. Cell Dev. Biol. **20**, 839 (2004).
[12] K. Simons and W. Vaz, Annu. Rev. Biophys. Biomol. Struct. **33**, 269 (2004).
[13] A. Kusumi, C. Nakada, K. Ritchie, K. Murase, K. Suzuki, H. Murakoshi,

R. Kasai, J. Kondo, and T. Fujiwara, Annu. Rev. Biophys. Biomol. Struct. **34**, 351 (2005).

[14]C. Dietrich, B. Yang, T. Fujiwara, A. Kusumi, and K. Jacobson, Biophys. J. **82**, 274 (2002).

[15]G. Vereb, J. Szollosi, J. Matko, P. Nagy, T. Farkas, L. Vigh, L. Matyus, T. Waldmann, and S. Damjanovich, Proc. Natl. Acad. Sci. U.S.A. **100**, 8053 (2003).

[16]E. Sackmann, Science **271**, 43 (1996).

[17]L. Tamm and H. McConnell, Biophys. J. **47**, 105 (1985).

[18]C. M. Ajo-Franklin, P. V. Ganesan, and S. G. Boxer, Biophys. J. **89**, 2759 (2005).

[19]V. Kiessling and L. Tamm, Biophys. J. **84**, 408 (2003).

[20]B. Koenig, S. Krueger, W. Orts, C. Majkrzak, N. Berk, J. Silverton, and K. Gawrisch, Langmuir **12**, 1343 (1996).

[21]E. Evans and E. Sackmann, J. Fluid Mech. **194**, 553 (1988).

[22]A. Prasad, J. Kondev, and H. A. Stone, Phys. Fluids **19**, 113103 (2007).

[23]M. Tanaka and E. Sackmann, Nature (London) **437**, 656 (2005).

[24]M. Tanaka, J. Hermann, I. Haase, M. Fischer, and S. G. Boxer, Langmuir **23**, 5638 (2007).

[25]E. T. Castellana and P. S. Cremer, Surf. Sci. Rep. **61**, 429 (2006).

[26]A. N. Parikh and J. T. Groves, MRS Bull. **31**, 507 (2006).

[27]M. L. Longo and C. D. Blanchette, Biochim Biophys Acta-Biomemb. **1798**, 1357 (2010).

[28]S. Bhat, S. Spitalnik, F. Gonzalez-Scarano, and D. Silberberg, Proc. Natl. Acad. Sci. U.S.A. **88**, 7131 (1991).

[29]J. Fantini, D. Cook, N. Nathanson, S. Spitalnik, and F. Gonzalez-Scarano, Proc. Natl. Acad. Sci. U.S.A. **90**, 2700 (1993).

[30]P. Clapham, A. McKnight, S. Talbot, and D. Wilkinson, Perspect. Drug Discovery Des. **5**, 83 (1996).

[31]K. Simons and G. Van Meer, Biochemistry **27**, 6197 (1988).

[32]K. Suzuki, J. Child Neurol. **18**, 595 (2003).

[33]D. Wenger, M. Sattler, and W. Hiatt, Proc. Natl. Acad. Sci. U.S.A. **71**, 854 (1974).

[34]T. Thompson and T. Tillack, Annu. Rev. Biophys. Biomol. Struct. **14**, 361 (1985).

[35]D. Brown and J. Rose, Cell **68**, 533 (1992).

[36]C. D. Blanchette, W. C. Lin, T. Ratto, M. McElfresh, and M. Longo, Biophys. J. **88**, 73a (2005).

[37]C. D. Blanchette, W. C. Lin, T. V. Ratto, and M. L. Longo, Biophys. J. **90**, 4466 (2006).

[38]C. Blanchette, W. Lin, C. Orme, T. Ratto, and M. Longo, Langmuir **23**, 5875 (2007).

[39]C. Blanchette, W. Lin, C. Orme, T. Ratto, and M. Longo, Biophys. J. **94**, 2691 (2008).

[40]D. Ducharme, J. Max, C. Salesse, and R. Leblanc, J. Phys. Chem. **94**, 1925 (1990).

[41]M. Howland, A. Szmodis, B. Sanii, and A. Parikh, Biophys. J. **92**, 1306 (2007).

[42]R. M. A. Azzam and N. M. Bashara, *Ellipsometry and Polarized Light* (North-Holland, Amsterdam, 1987), p. 1, 539.

[43]S. Faiss, S. Schuy, D. Weiskopf, C. Steinem, and A. Janshoff, J. Phys. Chem. B **111**, 13979 (2007).

[44]D. E. Aspnes, Surf. Sci. **101**, 84 (1980).

[45]A. Szmodis, C. Blanchette, A. Levchenko, A. Navrotsky, M. Longo, C. Orme, and A. Parikh, Soft Matter **4**, 1161 (2008).

[46]J. Petrov, T. Pfohl, and H. Möhwald, J. Phys. Chem. B **103**, 3417 (1999).

[47]M. Thoma, M. Schwendler, H. Baltes, C. Helm, T. Pfohl, H. Riegler, and H. Möhwald, Langmuir **12**, 1722 (1996).

[48]R. Horvath, G. Fricsovszky, and E. Papp, Biosens. Bioelectron. **18**, 415 (2003).

[49]A. Parikh and D. Allara, J. Chem. Phys. **96**, 927 (1992).

[50]A. F. Xie, R. Yamada, A. A. Gewirth, and S. Granick, Phys. Rev. Lett. **89**, 246103 (2002).

[51]T. Witten and L. Sander, Phys. Rev. B **27**, 5686 (1983).

[52]E. Sørensen, H. Fogedby, and O. Mouritsen, Phys. Rev. Lett. **61**, 2770 (1988).

[53]W. Curatolo, Biochemistry **24**, 6608 (1985).

[54]D. Marsh, A. Watts, and P. Knowles, Biochim. Biophys. Acta **465**, 500 (1977).

[55]B. Zimm and J. Bragg, J. Chem. Phys. **31**, 526 (1959).

[56]F. Tokumasu, J. Electron Microsc. **51**, 1 (2002).

[57]D. Needham and E. Evans, Biochemistry **27**, 8261 (1988).

[58]P. G. Debenedetti and F. H. Stillinger, Nature (London) **410**, 259 (2001).

[59]A. Miller, W. Knoll, and H. Möhwald, Phys. Rev. Lett. **56**, 2633 (1986).

[60]B. Ohler, I. Revenko, and C. Husted, J. Struct. Biol. **133**, 1 (2001).

[61]A. Arnold, I. Cloutier, A. Ritcey, and M. Auger, Chem. Phys. Lipids **133**, 165 (2005).

[62]R. Oliveira, M. Tanaka, and B. Maggio, J. Struct. Biol. **149**, 158 (2005).

[63]J. A. Moran-Mirabal, D. A. Aubrecht, and H. G. Craighead, Langmuir **23**, 10661 (2007).

[64]S. Schuy and A. Janshoff, ChemPhysChem **7**, 1207 (2006).

[65]C. Blanchette, C. Orme, T. Ratto, and M. Longo, Langmuir **24**, 1219 (2008).

[66]M. Seul, S. Subramaniam, and H. M. McConnell, J. Phys. Chem. **89**, 3592 (1985).

[67]D. Keller, N. B. Larsen, I. M. Moller, and O. G. Mouritsen, Phys. Rev. Lett. **94**, 025701 (2005).

[68]A. Charrier and F. Thibaudau, Biophys. J. **89**, 1094 (2005).